1661-8726/09/010015-15
DOI 10.1007/s00015-009-1310-8
Birkhäuser Verlag, Basel, 2009

Swiss J. Geosci. 102 (2009) 15–29

Stability and isotopic dating of monazite and allanite in partially molten rocks: examples from the Central Alps

Alfons Berger [1, *], Claudio Rosenberg [2] & Urs Schaltegger [3]

Key words: allanite, monazite, Alps, single grain U/Pb dating, migmatites

ABSTRACT

We investigated the stability of monazite and allanite as a function of bulk rock composition within several types of Tertiary Alpine anatexites, characterized by different compositions and melting reactions, but similar P-T conditions of melting. The investigated rocks consist of: (1) orthogneisses in which the melting reaction was triggered by water infiltration from the Bergell pluton; (2) anatectic tonalites, which were affected by water-assisted melting; and (3) metapelitic migmatites, which underwent muscovite dehydration melting. The studied anatexites cover a large range of Ca contents and water activities during partial melting, and allow an assessment of how much these parameters affect the stability of accessory phases. The different melting reactions that affected these rocks generated different water activities during the melt-present stage; they were highest in the water-saturated, contact metamorphic anatexites, and lowest in the metapelitic anatexites that underwent dehydration melting. These differences go together with different accessory phases within the migmatites. Whereas metapelitic anatexites only contain monazite, anatexites derived from tonalitic and granodioritic protoliths mainly contain allanite. This is consistent with observations made on Tertiary Alpine anatexites, suggesting that the growth of specific accessory phases is determined by the water activity and Ca content during melting.

We measured single-grain monazite U/Pb isotope ages. One grain has relics of old cores, which have also been detected in Y-zonation patterns of the monazite. The data of unzoned monazites indicate partial melting in the Southern Steep Belt between 30.78 ± 0.14 and 28.10 ± 0.28 Ma.

Introduction

The stability of accessory minerals is a key to understand the geochemical evolution of crustal rocks during melting and crystallization, because REE are almost completely hosted in these minerals (e.g., Miller & Mittlefehldt 1982; Watt et al. 1996). Some of these minerals, e.g., allanite, zircon and monazite, are frequently used geochronometers; hence a good petrologic constraint on their formation has important implications for the correct interpretation of isotopic ages. Whereas analytical errors of age determinations have become increasingly small, the geologic interpretation of these isotopic ages still remains uncertain, because the criteria relating a specific geologic event to a measured datum are generally lacking. The problem concerns the distinction between mineral phases formed during melting or during crystallization of migmatites. This distinction is fundamental when dating these minerals from migmatites, because the long residence time of melt in the deeper crust (10^6–10^7 yr, Rosenberg et al. 2007) makes it difficult to attribute the analytically precise ages to a specific geologic process within a long-lasting period of crustal melting. Better constraints on the phase relationships of accessory minerals are needed before isotopic ages can be accurately coupled to specific, possibly short, intervals of a P-T path.

Recent studies controversially discussed the effects of temperature and bulk chemistry on the phase stability of monazite and allanite (e.g., Rasmussen, 2006). Whereas the investigations on metamorphic rocks emphasised the role of temperature on the stability of these accessory phases, the effect of Ca was stressed as a controlling factor within magmatic systems. In metapelitic systems, several investigations indicate that the transition from monazite to allanite and back to monazite occurs between low grade and amphibolite grade conditions (Smith & Barreiro 1990; Wing et al. 2003; Tomkins & Pattison 2007; Janots et al. 2007, 2008). In addition to the temperature, the Ca content is known to play a

[1] Institute of Geology, University of Bern, Baltzerstrasse 1+ 3, 3012 Bern, Switzerland and Institute of Geography and Geology, University of Copenhagen, Østervoldgade 10, DK-1350 Copenhagen, Denmark.
[2] Freie Universität Berlin, Fachbereich Geowissenschaften, D-12249 Berlin, Germany.
[3] Département de Minéralogie, University of Geneva, Rue des Maraîchers 13, CH-1205 Genéve, Switzerland.
*Corresponding author: Alfons Berger. E-mail: ab@geo.ku.dk.

major role in the stability of monazite and allanite (e.g., Wing et al. 2003, Janots et al. 2008). Within magmatic rocks, where the crystallization temperature of monazite and allanite are relatively close (e.g., Lee & Silver 1964; Casillas et al. 1995), the Ca content is the factor determining which of these accessory phases is stable. Indeed, the occurrence of allanite inclusions within monazite has been attributed to changing Ca activity during the crystallization of granite (Broska et al. 2000). In addition, monazite is widespread in peraluminous, Ca-poor granitoids, whereas allanite and titanite dominate in calc-alkaline granitoids (e.g., Lee & Silver 1964). Migmatites are suitable for a combined study, where the role of temperature and composition (e.g. Ca content) on the stability of monazite and allanite can be tentatively assessed. Migmatites consist of alternating rock portions of different compositions on the scale of hand specimens (mesosomes, melanosomes and leucosomes). Despite the variable compositions of the protoliths, the newly formed partial melts are relatively similar in composition (Johannes & Holtz 1996 and literature therein). A better understanding of the stability of allanite and monazite requires new thermodynamic data (Janots et al. 2007), but petrographic data on natural samples are also helpful (e.g., Petrik et al. 1995; Franz et al. 1996; Förster 1998; Förster et al. 1999; Bea & Montero 1999; Broska et al. 2000).

The aim of this contribution is twofold: (1) we investigate the influence of the bulk composition and the fluid content on the stability fields of monazite versus allanite by comparing the occurrence and texture of these phases in migmatitic rocks affected by similar P-T conditions, but having different bulk compositions; (2) we use these petrological results to draw some conclusions about the preservation of allanite and monazite during partial melting, and about the preservation of isotopic ages older than the anatectic event. We test these results with single-grain monazite ages in the Central Alps, where previous age determinations on other mineral phases can help to assess the meaning of our monazite U-Pb ages from migmatites and to validate our interpretation.

Geological setting and sample descriptions

The studied anatexites are exposed in two areas of the Central Alps. One area is located in a tectonic window at the base of the Bergell Pluton (Fig. 1; Berger et al. 1996), where contact metamorphism induced partial melting in the immediate vicinity of the pluton. A second area is part of the Southern Steep Belt (SSB; Fig. 1), where Tertiary regional metamorphism locally induced partial melting within a lithologically heterogeneous series.

Migmatites from the Bergell area

The Bergell pluton is a deep-seated, calc-alkaline intrusion, syntectonically emplaced along a nappe boundary, between Penninic and Australpine units (Fig. 1; Rosenberg et al. 1995; Berger et al. 1996). A tectonic window (e.g., Davidson et al. 1996) exposes the base of the pluton and its migmatised country rocks. Within these rocks of granodioritic composition, biotite is the only rock-forming Fe-Mg mineral in the restite and in the protolith, indicating that melting did not involve this hydrous phase. In addition, the lack of phases related to incongruent melting (see detailed discussions in Rosenberg & Berger 2001, Berger & Rosenberg 2003 and Berger et al. 2008) suggests that melting occurred by a fluid-assisted reaction and not by dehydration melting. In these rocks melting results from infiltration of a free aqueous fluid, which attacked plagioclase, quartz and K-feldspar. Based on thermal modelling of the contact metamorphism (Trommsdorff & Connolly 1996) and on the absence of dehydration melting reactions, the melting temperature is constrained to approximately 700 °C (Johannes & Holtz 1996; Rosenberg & Berger 2001).

The protolith as well as the leucosomes and residues of these anatexites are exposed in structural continuity (Rosenberg & Berger 2001). In the following, we describe the composition of these rocks with special emphasis on the occurrence, fabric and composition of the accessory minerals. Detailed textural and compositional descriptions of the major and minor element chemistry of the bulk rocks BM5, BM6, BM7, BM8 and BM17 are given by Berger and Rosenberg (2003); see also Tables 1, 2.

The protolith is an augengneiss consisting of K-feldspar, plagioclase, quartz, biotite and ilmenite. The X_{Mg} (Mg/Mg + Fe) of biotite is ~0.37, and the TiO_2 content is close to 3 wt% (Table 1). The main accessory minerals are allanite, zircon and apatite, whereas monazite is absent. The allanites are 400–750 μm in size and some grains show patchy zonation. They are characterized by ∑REE of 18.3–24.4 wt% and by ThO_2 contents of 1.5–1.7 wt% (Table 3). Locally, small inclusions (<10 μm) with a composition corresponding to huttonite and thorite (see Table 4 for mineral analyses) are hosted in the allanites (Fig. 2). These inclusions occur as a single-phase or as symplectitic intergrowths with apatite (Fig. 2). The leucosomes are dominated by quartz, plagioclase and alkali-feldspar. Biotite is rare in comparison to the meso- and melanosomes. The X_{Mg} of biotite is higher with respect to the protolith, whereas the TiO_2 content is similar to the remaining parts of the anatexite. Accessory minerals are zircon, apatite and monazite. In contrast to the protolith, allanite is absent. The residue is enriched in biotite and plagioclase whereas alkali-feldspar is rare or absent. Plagioclase has higher An contents compared to the protolith and leucosome (Table 1; Rosenberg & Berger 2001). Accessory minerals are mainly monazite, allanite, apatite, zircon and occasionally xenotime. The amounts of monazite, apatite and zircon are higher than in the protolith as indicated by higher concentrations of REE (Berger & Rosenberg 2003; their Fig. 9a). Monazite, which is the main LREE mineral, is locally overgrown or replaced by allanite (see Fig. 2b). The Th content of these allanites ranges between 0.1 and 1.4 wt% (see Table 3) and their textures suggest a reaction of monazite to allanite (Fig. 2b).

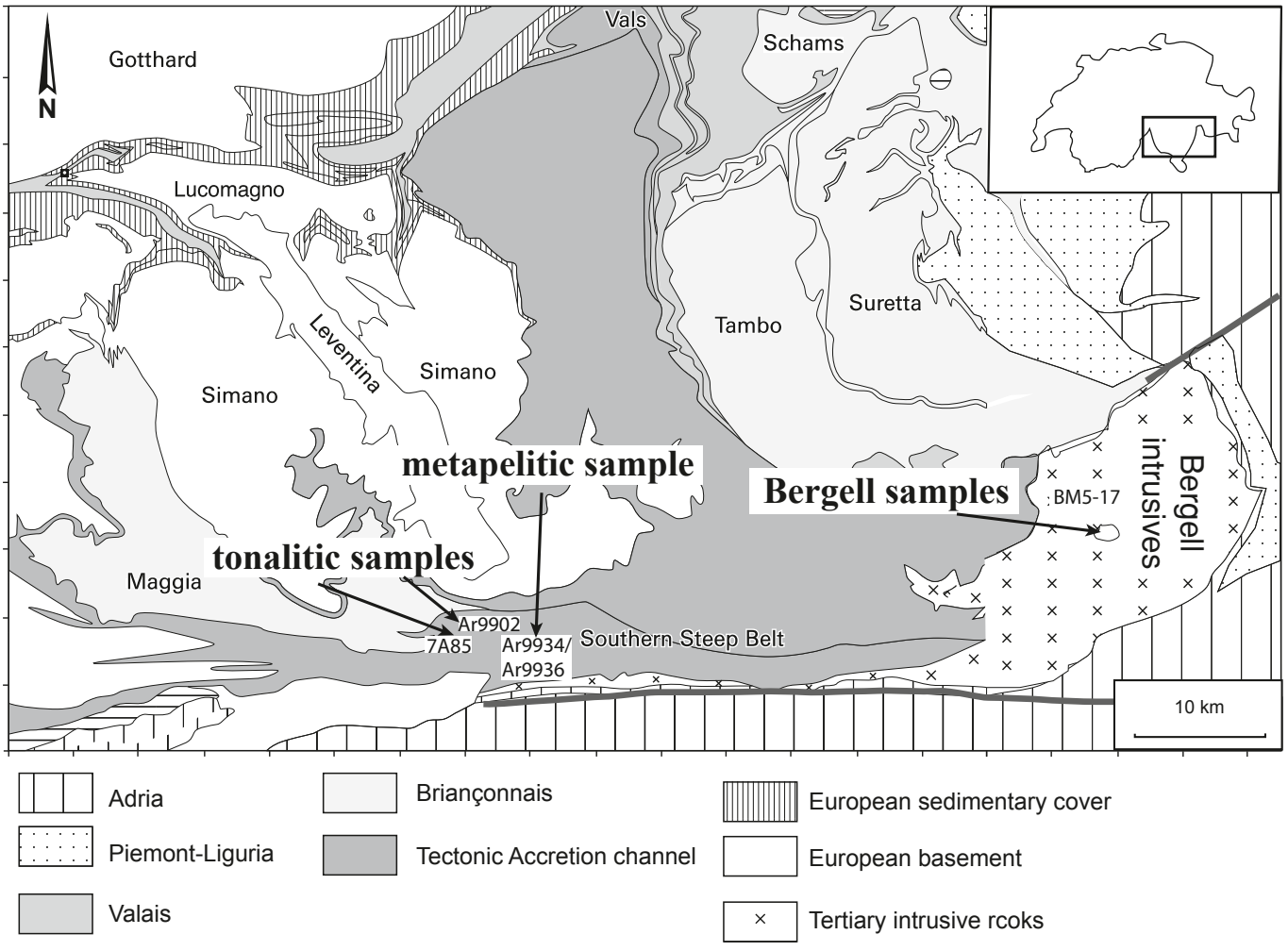

Fig. 1. Simplified tectonic map of the Central Alps (Switzerland/Northern Italy) showing sample locations (see also Table 1).

Table 1. Used samples and their major characteristics.

Sample	Swiss coord. x	Swiss coord. y	Part of the Migm.	Rock-forming minerals present in addition to Qtz + Bt	Rock group of the protolith	Loc.	LREE minerals	CaO content [wt%]	Reference
Ar9936L	728.1	117.9	Leuco	Pl, Kfs, Sill	Metapelitic migmatite	SSB	Mnz	2.7	Berger et al. 2005
Ar9936M			Meso	Pl, Kfs, Grt, Sill			Mnz	1.73	
Ar9934			Proto	Pl, Kfs, Sill			Mnz		
7A85L	725.5	118.8	Leuco	Pl, Hbl	Tonalitic migmatite	SSB	Aln	3.88	this study
7A85M			Meso	Pl, Hbl			Aln	4.27	
Ar9902L	725.1	119.3	Leuco	Pl, Kfs, Hbl			Aln	2.87	Burri et al. 2005
Ar9902M			Meso	Pl, (Kfs), Hbl			Aln	4.68	
BM5	766.0	123.9	Leuco	Pl, Kfs	Granitic-grano-dioritic anatexites	Bergell area	Mnz	1.7	Berger & Rosenberg 2003; Rosenberg & Berger 2001
BM6			Melano	Pl			Aln	4.1	
BM7			Proto	Pl, Kfs			Aln	2.65	
BM8			Proto	Pl, Kfs			Aln	2.71	
BM17			Melano	Pl			Mnz/Aln	4.19	

Abbrevations: leuco: leucosome, meso: mesosome, proto: protolith, melano: melanosome, aln: allanite; mnz: monazite.

Table 2. Bulk rock chemistry of samples used. All major elements in wt%, trace element in ppm.

Sample Type LREE-min.	Ar9936L leuco Mnz	Ar9936M meso Mnz	BM7 protho Aln	BM5 leuco Mnz	BM6 Klast melano Aln	7A85L leuco –	7A85M meso Aln	Ar9902L (leuco) Aln	Ar9902M (meso) Aln
SiO_2	66.29	58.29	71.70	73.17	59.43	66.46	58.24	67.80	58.83
TiO_2	0.54	1.22	0.21	0.20	0.88	0.33	0.75	0.46	0.86
Al_2O_3	16.23	17.12	15.55	14.59	19.18	15.59	18.27	15.39	16.98
Fe_2O_3	3.71	8.66	1.63	1.62	6.07	2.70	6.20	2.87	6.53
MnO	0.05	0.11	0.03	0.04	0.09	0.04	0.09	0.06	0.16
MgO	1.43	3.35	0.44	0.48	1.64	1.24	2.90	1.15	2.90
CaO	2.70	1.73	2.65	1.70	4.10	3.88	4.27	2.87	4.68
Na_2O	3.76	2.13	4.35	3.80	5.11	3.84	3.86	3.50	3.96
K_2O	1.82	3.70	2.60	4.14	2.19	1.64	2.80	3.43	2.26
P_2O_5	0.20	0.24	0.05	0.07	0.28	0.06	0.09	0.11	0.21
LOI	0.64	0.91	0.25	0.21	0.44	0.35	0.67	0.41	0.56
SUM	97.36	97.45	99.46	100.01	99.40	96.12	98.15	98.02	97.93
Ba	389	698	979	1098	500	320	381	651	150
Rb	58	141	62	112	124	43	109	89	93
Sr	297	171	385	330	402	279	279	347	294
Y	22	41	12	18	38	11	6	20	22
Zn	46	100	51	45	114	45	99	51	180
Zr	100	226	152	137	371	69	96	153	186

Fe(tot) measured as Fe_2O_3.

Migmatites from the Southern Steep Belt (SSB)

The SSB (Fig. 1) consists of peridotites, amphibolites, orthogneisses and metapelites, all displaying a strong, uniform fabric (e.g., Engi et al. 2001), acquired under amphibolite facies conditions and largely preserved without a retrograde overprint. Migmatites of Alpine age locally occur in the SSB. They contain discordant leucosomes as veins and patches which preserve magmatic fabrics and point to crystallization from a partial melt. The metamorphic conditions of partial melting were estimated at ~700 °C and 0.7–0.8 GPa (Burri et al. 2005). Within the SSB we investigated two types of anatexites, one of primary tonalitic-granodioritic, and one of primary pelitic composition.

Migmatites with tonalitic protolith

Two different samples were investigated, which are located relatively close together (samples Ar9902, 7A85; see Table 1). The leucosomes of these rocks consist of plagioclase, quartz and minor amounts of K-feldspar and amphiboles. The mesosomes are rich in biotite, plagioclase and amphibole (Fig. 3a). The amphiboles are homogeneous in composition with X_{Mg} of 0.5 to 0.53 and do not show any systematic compositional change between meso- and leucosome. Occurrences of amphibole in partially molten rocks are described from different places (e.g., Büsch et al. 1974; Mogk 1992), and experimental data show that this phase is only stable under water-assisted melting conditions (Gardien et al. 2000). Hence we interpret the amphiboles as incongruent reaction products of water-assisted melting (Gardien et al. 2000; Berger et al. 2008). Such a reaction can be written as:

$$\text{Biotite + Plagioclase (I) + Quartz + } H_2O \text{ (in fluid)} = \text{Hornblende + Plagioclase (II) + melt} \quad (1)$$

Allanite is the most common accessory mineral, and its abundance is higher than in the Bergell anatexites (Fig. 3b). Zircon and apatite are also present, whereas monazite is completely absent. The Th and REE contents of allanite are relatively low (Table 3; Fig. 3b).

Migmatites with pelitic protolith

In close proximity, migmatites also occur which have a metasedimentary protolith. The rocks are characterized by biotite, quartz, two feldspars, garnet and/or sillimanite. This characteristic mineralogy reflects the bulk-rock composition showing elevated Al and intermediate Ca contents (Tables 1 and 2). The physical conditions of melting are inferred to be similar to the aforementioned Ca-rich rocks, because they are only a few hundreds of meters apart and no faults separate them. The melanosomes are dominated by biotite and minor amounts of

Table 3. Selected allanite analyses.

Sample Location	BM17 Bergell-area residue	BM17 Bergell-area	BM8 Bergell-area protholith	BM8 Bergell-area	7A85 SSB
P_2O_5	0.02	0.04	0.03	0.03	0.01
SiO_2	33.68	31.45	32.60	30.91	36.86
ThO_2	0.09	1.41	1.45	1.71	0.19
UO_2	0.04	0.05	0.05	0.01	0.04
TiO_2	0.19	0.25	0.37	0.98	0.15
Al_2O_3	19.40	16.76	17.64	14.13	23.51
CaO	14.15	9.67	12.26	9.43	20.01
MgO	0.55	1.08	0.72	1.39	0.26
MnO	0.70	1.00	0.99	0.99	0.28
PbO	bdl	bdl	bdl	bdl	bdl
Fe_2O_3	14.50	15.02	15.41	16.36	12.53
Y_2O_3	0.71	0.25	1.01	0.38	0.51
La_2O_3	3.29	5.50	4.38	5.88	1.17
Ce_2O_3	7.23	11.58	8.22	11.81	2.35
Pr_2O_3	0.88	1.11	0.87	1.12	0.25
Nd_2O_3	3.09	4.50	3.17	4.28	1.10
Sm_2O_3	0.77	0.56	0.65	0.66	0.24
Gd_2O_3	0.54	0.30	0.56	0.39	0.21
Dy_2O_3	0.25	0.03	0.22	0.13	0.05
Ho_2O_3	0.05	0.02	0.07	0.03	0.01
Er_2O_3	0.10	0.09	0.14	0.10	0.06
Na_2O	0.03	0.08	0.03	0.06	na
Cl^-	0.01	0.01	0.01	0.01	na
Total	100.30	100.81	100.82	100.82	99.79
ΣREE + Th (wt%)	16.29	25.08	19.71	26.12	5.63

garnet and plagioclase (Fig. 3d), whereas the leucosomes are dominated by K-feldspar, plagioclase and quartz. Aluminosilicates occur in both portions of the migmatite. The compositional range of the plagioclase overlaps between leucosomes and mesosomes (see different situation in the Bergell migmatites). The similar plagioclase compositions in leucosomes and mesosomes are most likely related to the crystallization processes in these migmatites. The growth of aluminosilicates combined with the occurrence of K-feldspar-rich leucosomes suggests a dehydration-melting reaction of the following type:

Muscovite + Biotite + Quartz + Plagioclase (I)
= Garnet + Plagioclase (II) + melt ± Aluminosilicate (2)

Monazite and apatite are common both in the meso- and melanosome. The Th content of monazite is ~2.2 wt% (Table 4). In the leucosomes, monazite is also the stable LREE phase and allanite is absent in all parts. The mesosomes of these samples are rich in apatite and also contain zircon (Fig. 3d).

Results

Analytical procedures

The mineral chemistry of allanite, huttonite and monazite has been analysed with a Cameca SX50 electron microprobe, at operating conditions of 25 kV and 50 nA. The following elements were measured: Na(Kα), Mg(Kα), Al(Kα), Si(Kα), P(Kα), Ca(Kα), Ti(Kα), Cr(Kα), Mn(Kα), Fe(Kα), Sr(Lα), Y(Lα), Pr(Lβ), Ce(Lα), La(Lα), Sm(Lβ), Nd(Lβ), Dy(Lβ), Gd(Lβ), Ho(Lβ), Er(Lα), Th(Mα) and Pb(Mα). Overlapping of peaks has been tested with VirtualWDS (Reed & Buckley, 1996). Background positions have been carefully chosen after testing with VirtualWDS. Different oxides, phosphates and silicates have been used as standard materials. Counting times on peak and background ranged between 20 s and 80 s. Counting times of 200 s were used for Pb in huttonite (for technical details see Scherrer et al. 2000). The rock forming silicates were measured with 15 kV and 20 nA with silicate

Table 4. Representative monazite and Th-silicate analyses.

Sample	Ar9936	Ar9936	BM17	BM8
Type	residue	residue	residue	proth
Mineral	mnz	mnz	mnz	Th-silicate
P_2O_5	30.27	30.75	28.30	3.56
SiO_2	0.36	0.37	1.54	16.48
ThO_2	3.44	2.97	6.60	67.00
UO_2	0.69	0.75	0.74	2.93
CaO	0.95	0.79	0.78	0.23
Fe_2O_3			0.29	0.22
Y_2O_3	0.54	2.67	1.46	1.03
La_2O_3	16.84	14.56	14.31	1.57
Ce_2O_3	30.20	28.04	28.74	4.04
Pr_2O_3	3.03	3.00	3.16	0.32
Nd_2O_3	10.88	11.72	11.91	1.91
Sm_2O_3	1.54	2.02	1.67	0.39
Gd_2O_3	0.95	1.65	1.05	0.38
Dy_2O_3	0.23	0.74	0.38	0.30
Ho_2O_3	bdl	0.08	0.01	0.03
Er_2O_3	0.05	0.16	0.10	0.09
PbO	bdl	bdl	bdl	0.07
Total	100.04	100.45	101.03	100.54

and oxide standards, and a counting time of 20 s. PAP corrections have been applied to raw data. Monazite single grain isotope data were measured with isotope-dilution thermal ionization mass-spectrometry (for analytical procedure see Schaltegger et al. 2005).

Bulk rock contents of Sr, Rb, Ba, Pb, Ni, V, Zr, Zn and Y were determined by standard X-ray fluorescence on glass pellets. Whole-rock REE values were obtained by ICP-MS at Activation-Labs (Canada). The separation of leucosomes and mesosomes in hand specimens was done on structural criteria. Hence, the sample volumes were sometimes small.

Composition of accessory phases

The allanites of the protolith in the anatexite from the Bergell area have a relatively high Th content (~1.7 wt%) and their microstructure shows the exsolution of a Th-rich mineral with a high content of LREE (Fig. 4; Table 4). The measured composition of this mineral (see Table 4) is consistent with thorite or huttonite (both $ThSiO_4$). In general, Th contents of allanites commonly range between 0.2–1.7 wt% ThO_2, (e.g., Deer et al. 1982; Catlos et al. 2000; Wood & Ricketts 2000; Poitrasson 2002). The allanites from the protolith contain 1.4–1.7 wt% ThO_2 which is close to the maximum values of Th contents reported in the literature (see above; Fig. 4). The exsolution of Th into thoriumsilicate suggests also that these grains attained their maximum Th solubility. This is further supported by the high Th content in the allanites.

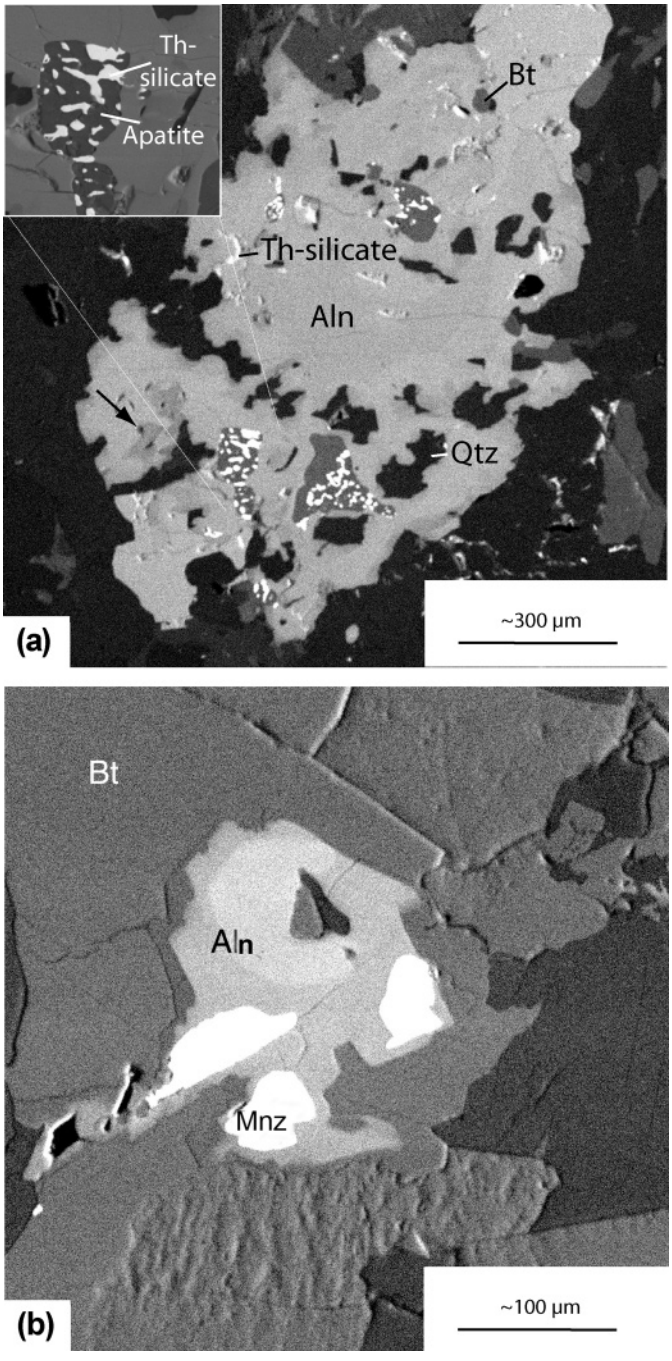

Fig. 2. (a) BSE photograph of allanite (Aln) in migmatite protolith of Bergell area showing small compositional changes (black arrow). Note the thorium silicate-apatite intergrowths within the allanite grain. One of these intergrowths is enlarged in the upper left corner of the figure. Other inclusions in the allanite are quartz (Qtz) and biotite (Bt). The size of the allanite grain is 0.5 mm. (b) BSE photograph of allanite (Aln) overgrowing or replacing monazite (Mnz) within a biotite (Bt) grain in the residue of the Bergell migmatites. These allanites are more concentrically zoned compared to allanite in the protolith.

Epidote/allanite in the tonalitic samples of the SSB is poor in REE and Th (samples Ar9902, 7A85; Table 3, Fig. 3b). These minerals are zoned from intermediate REE contents to pure

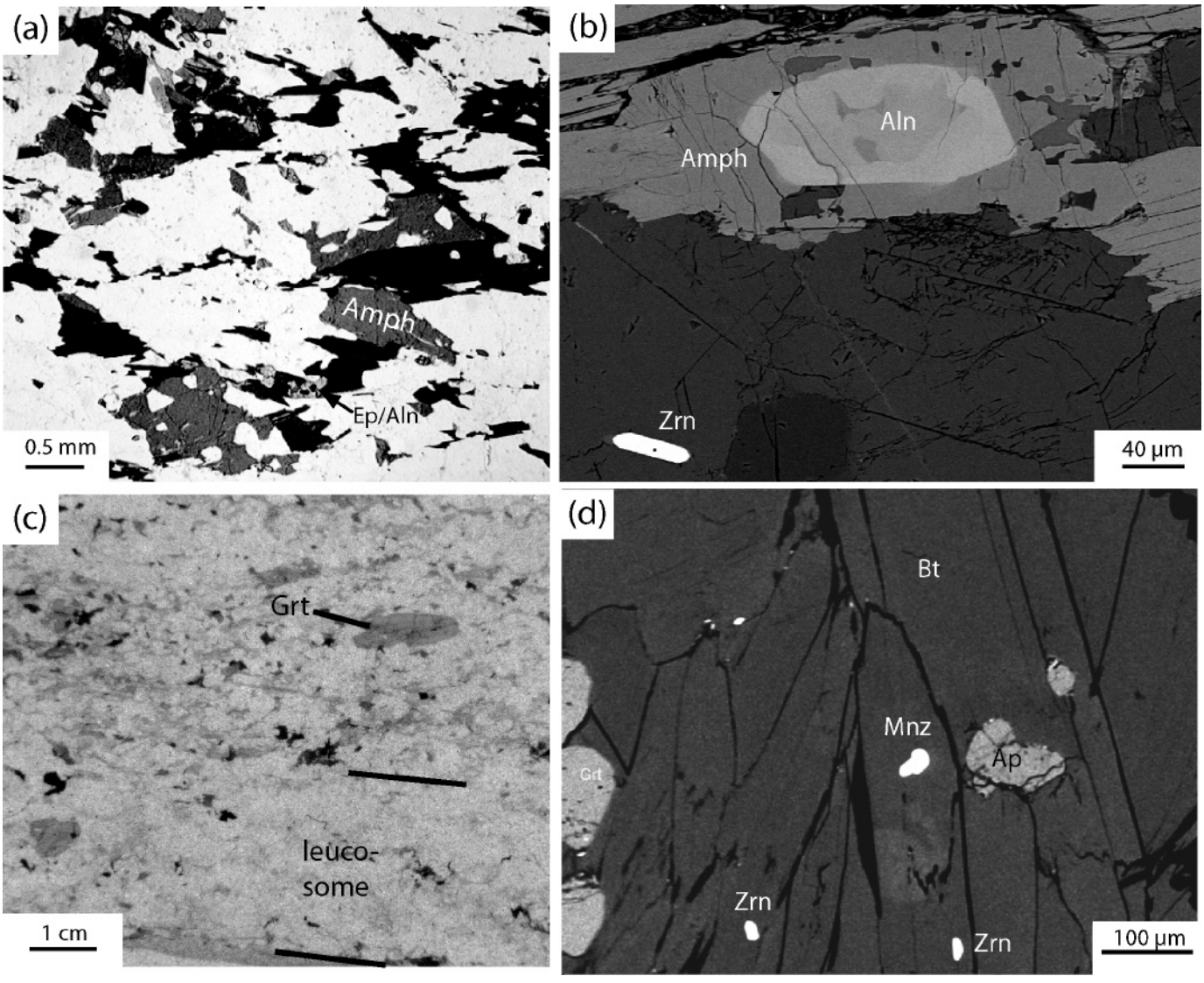

Fig. 3. Structures and microstructures of some samples. (a) Microphotograph of the amphibole-bearing migmatites in the SSB (sample Ar9902; plane polarized light). (b) BSE image of amphibole-bearing migmatite showing typical occurrence of allanite with zonation; surrounded by amphibole (sample 7A85). (c) Photograph of metapelitic migmatite (SSB, sample Ar9936). (d) BSE image of metapelitic migmatite (SSB, sample Ar9936) displaying high content of zircon, monazite and apatite in the mesosome of the restitic part.

epidote. Plotting these mineral compositions in a clinozoisite-epidote diagram (Fig. 4c), shows that the allanites from the tonalitic anatexites and the Bergell area are different. In the SSB migmatites, these minerals show a higher clinozoisite/ferriepidote ratio than in the Bergell samples. This mineral chemistry suggests that: (1) the modal abundance of the epidote group minerals controls the allanite component in the grains; (2) the higher clinozoisite/ferriepidote ratio indicates oxidizing conditions in the SSB samples (Fig. 4; cf. Petrik et al. 1995).

The composition of monazites in the migmatites from the Bergell area is homogeneous**.** In contrast, the monazites from the pelitic migmatites in the SSB exhibit variable Y contents. Several grains show high Y concentrations in the core and low Y at the rims, but the opposite has also been detected. The Y content in monazite depends on temperature (Pyle & Spear 2000, Pyle et al. 2001), and different Y contents have been related to different metamorphic stages (e.g., Pyle & Spear 2003). The variation in yttrium contents in our monazites may also be related to different metamorphic stages, which is consistent with the inheritance found by single grain isotope dating (see below; see also Berger et al. 2005).

Bulk rock composition

We measured the major and the trace element contents of the migmatites by separating them into macroscopically homoge-

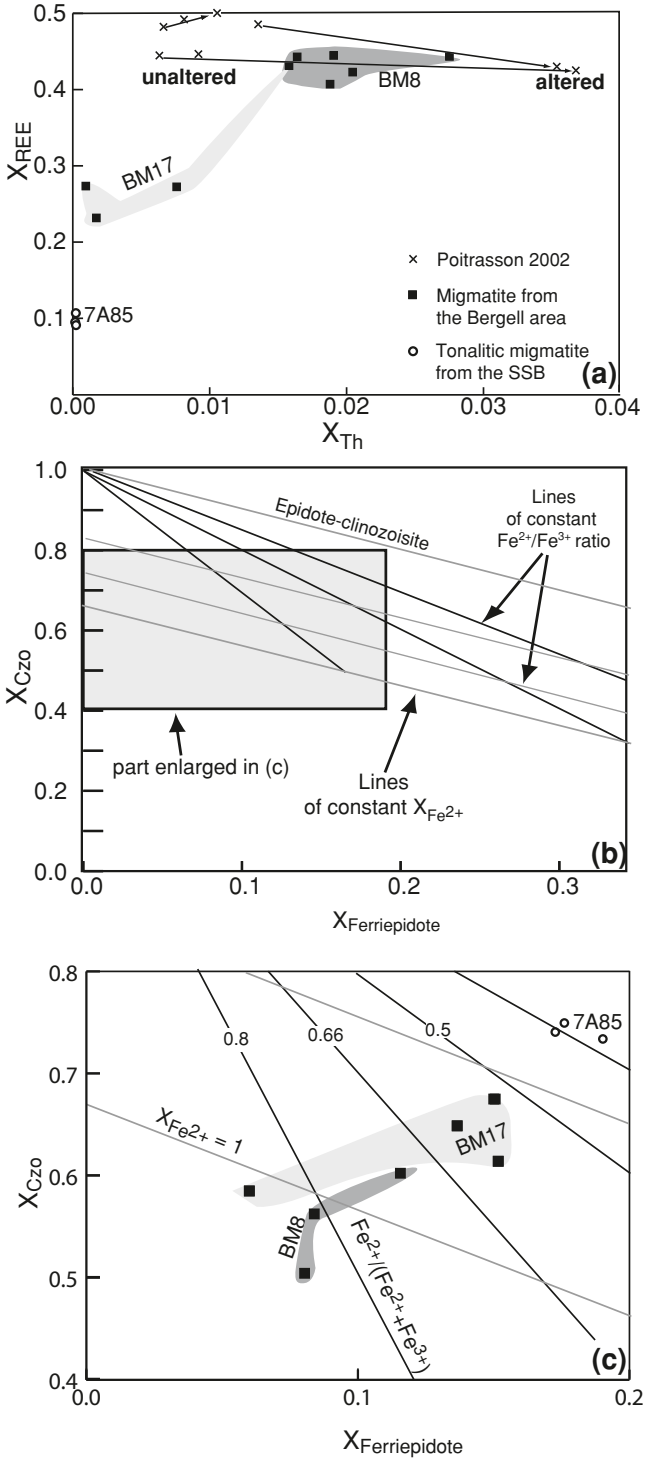

Fig. 4. Chemical composition of allanite. (a) Th contents of studied allanites in addition to compiled data in X_{Th} versus X_{REE} diagram (see Appendix for definitions). Data from Poitrasson (2002) are shown as example of hydrothermal alteration. (b) clinozoisite versus ferriepidote diagram (see Appendix for definitions). In this diagram, equilines of $Fe^{2+}/(Fe^{3+} + Fe^{2+})$ ratios can be calculated (bold lines). Our description of allanites allows also to indicate the amount $X_{Th} + X_{REE}$ in this diagram (thin grey lines) by ignoring the dissakisite component. (c) measured allanite composition in a clinozoisite versus ferriepidote diagram (see Fig. b for definitions and which section of the diagram is used). The data illustrate the varying Fe^{2+} and Fe^{3+} in the different grains.

Table 5. Isotope measurements.

Number	Weight [mg]	Concentrations				Atomic ratios						Apparent ages			Error corr.	207Pb/235U ages ± 2σ [Ma]
		U [ppm]	Pb rad. [ppm]	Pb nonrad. [pg]	Th/U [b]	206/204 [c]	207/235 [d]	Error 2σ [%]	206/238 [d]	Error 2σ [%]	207/206 [d]	206/238	207/235	207/206		
Ar9934-M6 [a]	0.0010	2549	28.91	9.9	5.61	94	0.02893	2.47	0.00460	0.45	0.04564	2.32	29.56	28.95	–	0.41	28.95 ± 0.70
Ar9936-M11 [a]	0.0010	1978	24.67	2.6	0.52	239	0.03421	2.03	0.00463	0.44	0.05361	1.89	29.77	34.16	354.84	0.42	34.16 ± 0.68
Ar9936/6	0.0089	3740	45.92	7.7	6.06	1359	0.03077	0.44	0.00490	0.34	0.04556	0.21	31.50	30.78	–	0.88	30.78 ± 0.14
Ar9936/11	0.0152	7284	78.24	30.5	5.40	1077	0.02837	0.54	0.00457	0.23	0.04506	0.46	29.37	28.41	–	0.53	28.41 ± 0.16
Ar9936/12	0.0062	6792	71.46	8.4	5.16	1498	0.02862	0.25	0.00459	0.23	0.04524	0.10	29.51	28.65	–	0.92	28.65 ± 0.07
Ar9936/13	0.0029	6137	64.37	97.4	5.32	71	0.02806	1.00	0.00448	0.23	0.04545	0.93	28.80	28.10	–	0.40	28.10 ± 0.28
Ar9936/14	0.0081	4676	50.28	6.1	5.30	1852	0.02862	0.25	0.00462	0.23	0.04496	0.10	29.70	28.66	–	0.92	28.66 ± 0.07

[a] Single monazite grains removed from thin section. [b] Calculated on the basis of radiogenic Pb^{208}/Pb^{206} ratios, assuming concordance. [c] Corrected for fractionation and spike. [d] Corrected for fractionation, spike, blank and common lead (Stacey & Kramers 1975).

neous volumes (i.e., leucosome, mesosome and melanosome; Table 2). Ca concentrations vary between different migmatites and also between the different parts of the same migmatite (Table 2). Although the absolute REE concentrations are different, all samples show similar REE patterns characterized by weak, positive or negative Eu anomalies. The major element concentrations have been used to compare bulk rock data with stable LREE phases (see section on stability of LREE minerals as function of Ca content).

Single-grain isotopic ages

In order to investigate the possible preservation of old accessory grains upon melting, we analysed the U-Pb isotopic composition of monazites from the metapelitic migmatites of the SSB (see also Table 5). We used two techniques to separate monazite grains from their matrix. Some grains were separated conventionally by crushing the rock samples and separating the monazites with heavy liquids. Two grains were drilled out of a thin section.

The weight of individual grains and the measured concentrations of U and Pb are shown in Table 5. The drilled grains have higher analytical errors caused by common lead contamination by the glue. The measured ages spread between 30.78 ± 0.14 and 28.10 ± 0.28 Ma (Fig. 5). One drilled-out grain shows a discordant U/Pb age, which result in apparent $^{206}Pb/^{238}U$ age of 29.77 Ma and a $^{207}Pb/^{235}U$ age of 34.16 ± 0.68 Ma (Table 5). The discordancy is interpreted to be related to the presence of a Y-rich core of an older age (Fig. 5). The other grains yield points above the concordia. This is related to preferential uptake of ^{230}Th during the growth leading to parentless excess ^{206}Pb (Schärer 1984). Crystallization of monazite in the presence of melt commonly produces grains that lie above the concordia (see Hawkins & Bowring 1999; Kalt et al. 2000). However, the geological meaning of these ages remains unclear, because the accessory phase of interest (i.e. monazite) is stable over a large time interval during metamorphism (e.g., Kelsey et al. 2008). Single grains (without inherited cores) may preserve the age of their prograde growth, the growth during the melting stage or retrograde reaction replacing other phases. Monazite grains that underwent some degree of Pb loss by diffusion or during retrograde recrystallization will be situated along a lead-loss trajectory in the concordia diagram, resulting in most cases in a normal discordancy below the concordia. Solid-state recrystallization of monazite during the retrograde path can be excluded, because this process should also affect other minerals, but no retrograde recrystallization textures are observed. Alternatively, these grains may be a product of solid reactions along the prograde path at lower temperatures. However, the missing reaction textures, as shown for the accessory phases in the Bergell migmatites, make this interpretation unlikely. Therefore, monazite ages obtained on metapelitic migmatites most likely yield the time of their crystallization during the migmatite stage.

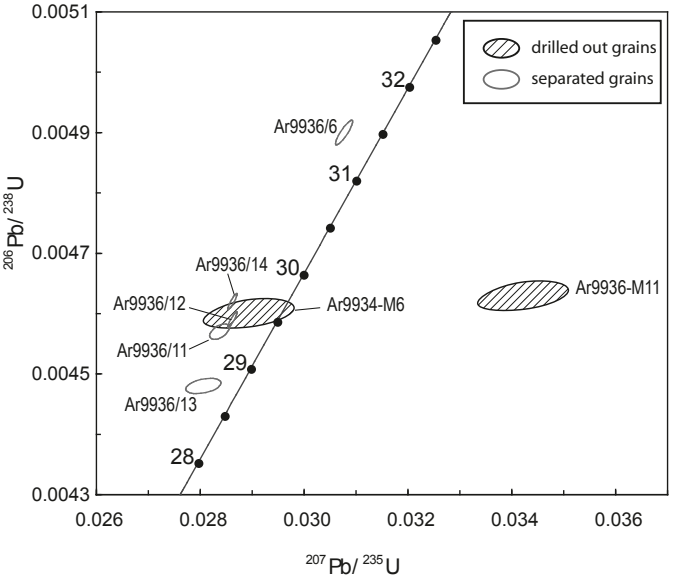

Fig. 5. U-Pb concordia diagram for monazite of the metapelitic migmatites of the Southern Steep Belt. The error ellipses represent 2σ analytical uncertainty. Dark ellipses are separated grains; labelled dark circles are drilled out grains.

Discussion

Stability and composition of LREE minerals as function of Ca content of the bulk rock

The role of bulk chemistry on the stability of monazite is under debate (see for example Wing et al. 2003; Fitzsimonis et al. 2005; Rasmussen et al. 2006; Janots et al. 2007, 2008). The samples of the present study are characterized by different compositions, but similar P and T conditions during melting. Therefore, comparing the occurrence of monazite and allanite, their textural relationships and isotopic signatures in the three groups of anatexites described above will give first indication of the phase relations between allanite and monazite. It has been proposed that the formation of monazite in metapelites depends on the type of metamorphic reactions, which in turn depend on the bulk composition, in particular on the Mg/Fe ratio and Al saturation in metapelites (e.g., Fitzsimonis et al. 2005). In contrast, in meta-granitoid systems, where the stability of accessory phases is controlled by Ca activity, the role of the feldspars may be more important than changes in the Mg/Fe ratio (see for example Broska et al. 2000).

In this study, we have the possibility to compare the occurrence of LREE phases in newly developed melt from different protoliths (mainly granitic) and mesosomes related to different protoliths. The bulk compositions of these different mesosomes are different, but comparable (see Fig. 6). In order to investigate the effect of Ca content on the stability of allanite in our sample series, we plotted the Ca/Si ratio of the bulk rock chemistry against (K + Na)/Al (Fig. 6a) as a proxy for their melting behaviour. This can be done, because melting mainly effects the quartz-feldspar components. The combination of figures 6a

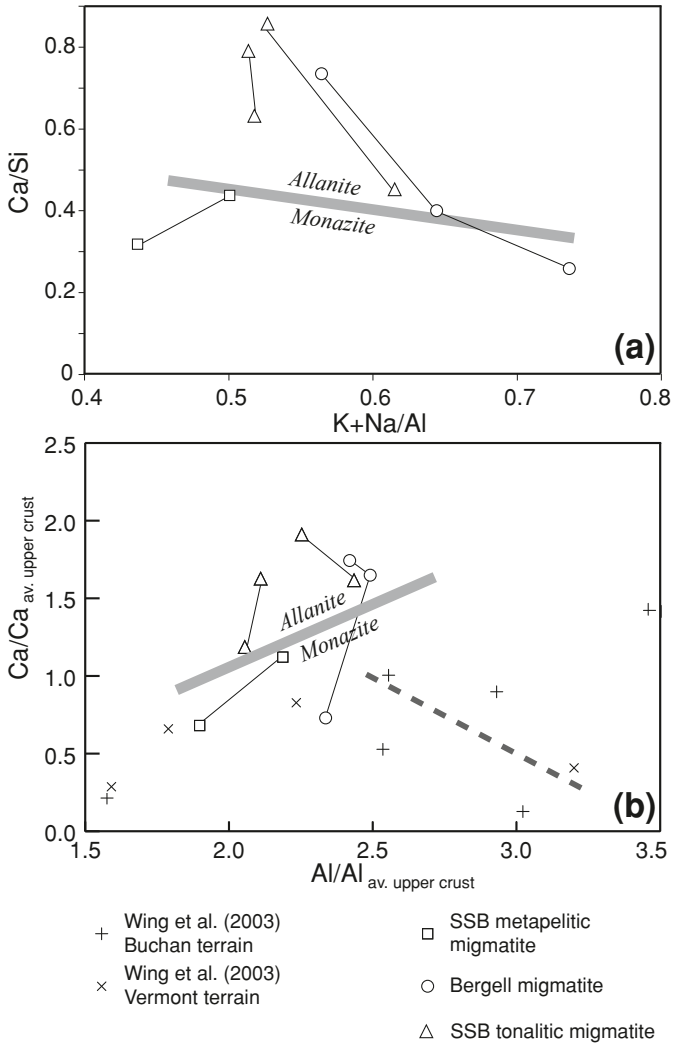

Fig. 6. Presentation of the bulk rock composition. (a) element ratio Ca/Si versus K + Na/Al of the whole rock composition. (b) Ca and Al content of the bulk rock composition normalized to average upper crust (http://georef.org). In addition data of Wing et al. (2003) are plotted. The bold grey lines divide allanite-dominated from monazite-bearing samples studied. The dashed grey line is the boundary found by Wing et al. (2003).

and 6b also shows the similarities of melts produced in different anatexites and the similarity of the mesosomes, despite the difference in protoliths. The similar compositions of the mesosomes in metasedimentary and metamagmatic rocks are caused by the relative high Ca content in the metasediments.

Previous studies on the role of bulk chemistry on the stability of monazite versus allanite concentrated on metasedimentary rocks (e.g., Wing et al. 2003; Fitzsimonis et al. 2005). In figure 6b the Ca content is plotted against the Al content of the whole rock (cf. Wing et al. 2003). In this figure, the stability limit of monazite and allanite is shown, which is slightly different to the proposal of Wing et al. (2003). The data from the migmatites represent the effect of Ca content expressed as the role of anorthite content in the feldspars (see Fig. 6). The presentation of phase stability in such a simple chemical projection may not help to understand the stability in P-T-X space. Several examples show a stronger effect of temperature rather than composition on the stability of monazite versus allanite (e.g., Rasmussen et al. 2006). The present study indicates the additional role of Ca and H_2O activity on this problem. A better understanding of the stability of accessory phases requires more complete P-T-X diagrams as shown by Janots et al. (2007).

However, the stability of accessory phases can be discussed within a chemical system consisting of CaO, FeO, Fe_2O_3, Al_2O_3, SiO_2, H_2O, REE_2O_3 and P_2O_5. The stability fields of the phases formed in such a system can be graphically illustrated using quartz and apatite as excess phases and the following components (Fig. 7a):

C: Ca
R: ΣREE + Y
A: Al
F: Fe^{3+}

In order to obtain a 2D representation, we have simplified this system by combining Fe^{3+} and REE (Figs. 7b–c). The stability fields of each investigated anatexite and those of the individual portions (leucosome, protolith and residue) of the Bergell area

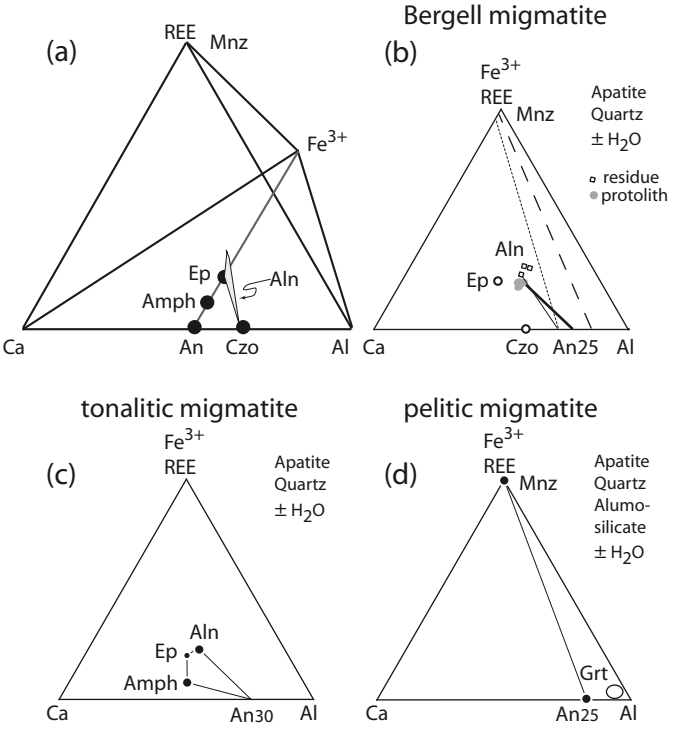

Fig. 7. Graphical presentation of REE-mineral composition with respect to Ca-Al content. (a) Tetrahedron showing location of considered epidote-group members. (b) Ca-Al-REE + Fe^{3+} triangle illustrating the paragenesis in leucosome (dotted line), residue (solid lines) and protolith (bold line) of the Bergell migmatites. (c) Paragenesis of tonalitic anatexites of the SSB in a Ca, Al and REE + Fe^{3+} triangle. (d) Ca, Al and REE + Fe^{3+} triangle showing the paragenesis of metapelitic anatexites in the SSB.

are shown in figure 7. In the Bergell anatexites, the tie lines of the protolith cut the tie lines of the residue (Fig. 7b), indicating that the residue became enriched in Ca. Considering that the compositions of allanites in the residue and protolith are similar (Table 3), we conclude that the Ca enrichment did not control the mineral chemistry of the allanites. The overgrowth of allanite on monazite in the residue (Fig. 3) indicates that monazite can be stable also at higher Ca contents. Therefore, in addition to Ca, other parameters such as water activity control the stability of the accessory phases.

Water activities at different stages of melting and crystallization

Monazite is a water-free phosphate, whereas allanite is a water-bearing silicate. Therefore, beside pressure and temperature, the stability of these minerals depends on water activity and oxygen fugacity (e.g., Schmidt & Thompson 1996 and Schmidt & Poli 2004 for epidote). In general, water activity during partial melting and crystallization evolves according to the following three stages:

1) pre-melting stage: water activity is determined by the composition of the free fluid phase.
2) melt-present stage: water activity is defined by the water dissolved in the melt and, if melt solubility is exceeded by the additional fluid phase (water solubility in melt depends mainly on pressure, which in this study is always the same). At this stage water activity is different in the different selected examples.
3) crystallization stage: water activity increases again due to the release of a free aqueous fluid from the crystallizing melt.

In the following, we qualitatively constrain water activities in each of the investigated migmatites in order to assess whether the occurrence of allanite and/or monazite is directly related to the water content during melting. Water activities in the anatexites of the Bergell aureole may be constrained with the aid of experimental results performed in the quartz-feldspar system (Johannes & Holtz 1996). Assuming that the water content needed to generate a given melt fraction in experiments is equal to the melt fraction generated in nature, one can estimate the melt fraction in nature and hence constrain the water content in comparison with the experimental results. The melt fraction formed during anatexis in the Bergell aureole is inferred to be 0.32 by subtracting the residue composition from the protolith composition (Berger & Rosenberg 2003). Excluding dehydration melting on the basis of petrographic evidence discussed above, such a melt fraction requires 6.5–7 wt% water at 0.6 GPa (Johannes & Holtz 1994).

The occurrence of amphibole as an incongruent melting product in the tonalitic anatexites of the SSB (samples 7A85, Ar9902) points to water-assisted melting (Gardien et al. 2000), hence lower water activities compared to water-saturated melting of the anatexites in the Bergell area. By analogy with experiments performed on similar rock compositions (Gardien et al. 2000), we infer that amphiboles and melt were stable at water contents of approximately 3 wt% in the bulk system. In the metapelitic rocks of the SSB (reaction 2), water was generated by the breakdown of hydrous phases during dehydration melting, and hence this water was immediately incorporated into the melt. Therefore, compared to the Bergell anatexites, the SSB rocks are inferred to have had the lowest water activity during melting.

Consequences of phase stability on geochemistry and geochronology

On the basis of the relationship between bulk composition, water activity, occurrence of specific accessory phases, and melting reaction of the migmatites investigated (Table 6), we distinguish the three following types of anatexites: (1) rocks with intermediate Ca contents, which underwent partial melting at high water activity (migmatites from the Bergell area), show a transition from the stability field of allanite to that of monazite upon melting; (2) Ca-rich rocks (tonalitic migmatites of the SSB), which underwent partial melting with intermediate or high water contents during the melting stage; and (3) rocks, which underwent dehydration melting (metapelitic migmatites of the SSB) at low water concentrations in the melting stage.

These three types of anatexites (Table 6) indicate that the stability of the accessory phases is influenced by the Ca content of local rock compositions and the water activity during melting and crystallization. In terms of resetting of isotopic systems and equilibration of LREE between accessoric phases, these rock types are expected to behave differently. Equilibration and age resetting are most effective in grains formed by mineral reactions. The nucleation and growth of new accessory phases is most likely in rocks with intermediate Ca contents (type 1: migmatites of the Bergell area) because the dominant LREE mineral (allanite) becomes unstable upon melting and leads to the new crystallization of monazite. In contrast, in migmatites of type 2 and 3, relicts of previous LREE-phases may survive during melting and crystallization. Therefore, age relics

Table 6. Comparison of the different investigated migmatites.

	Migmatite of the Bergell area Type 1	Tonalitic migmatite Type 2	Metapelitic migmatite Type 3
Bulk Ca-content	variable	high	intermediate
Water activity during melting	high	intermediate	low
Present phases	transition from allanite to monazite upon melting	only allanite	only monazite
Other observations	high Th content in allanite combined with Th-silicate	low REE and Th in allanite	rare inheritence in monazite

pointing to crystallization events preceding melting may occur in migmatites without phase transitions.

In the Bergell anatexites (type 1; Table 6), resetting of the accessory phases can only be inferred indirectly, because in-situ monazite and allanite ages are not yet available. However, the balance and distribution of trace elements between leucosome and residue in these rocks suggests that accessory phases such as allanite and monazite equilibrated upon melting (Berger & Rosenberg 2003). Therefore, preservation of relic ages in the accessory phases of these migmatites is not expected. In the metapelitic migmatites of the SSB (type 3), single grain isotopic data indicate the preservation of an inherited core, which is consistent with the interpretation that the variable yttrium contents are related to different metamorphic stages (Table 4). This yttrium zonation is most likely related to changes in temperature (Pyle et al. 2001), and indicates different metamorphic stages. The U-Pb data from one grain show that Variscan monazite grains can survive throughout the Alpine, high-temperature metamorphism in these types of migmatites (Fig. 5). This is consistent with the aforementioned interpretation, suggesting that accessory phases may not be completely destroyed if anatexis is driven by dehydration melting (see also Rubatto et al. 2001). Some monazites in metapelitic migmatite show a chemical and age zonation, in contrast to other grains which are homogeneous and are located above the concordia (Fig. 5). As discussed above, these data points indicate preferential uptake of Th during crystallization, and are most likely crystallization ages related to partial melting and crystallization (cf. Kalt et al. 2000).

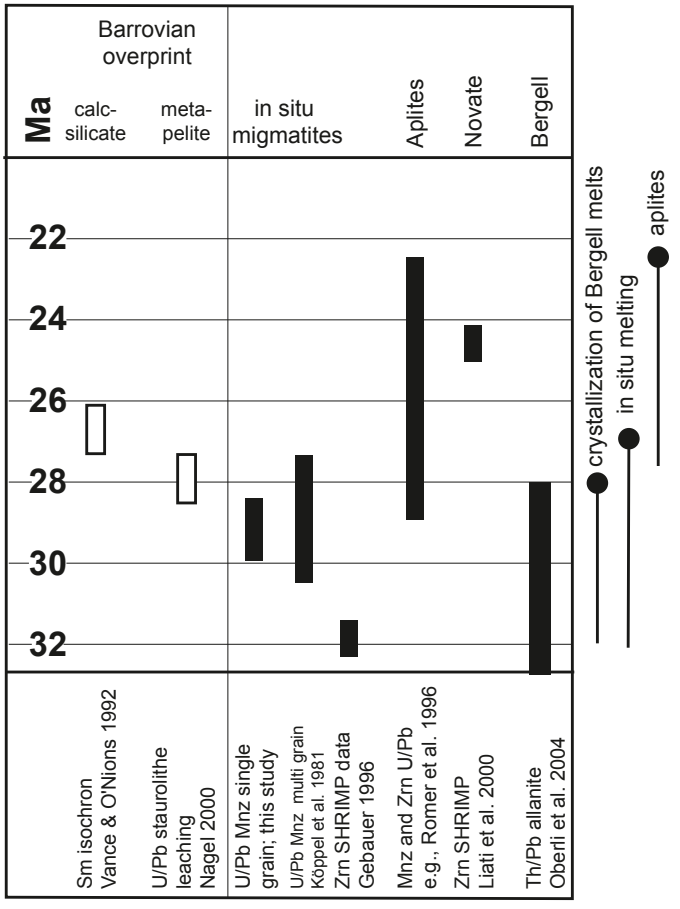

Fig. 8. Comparison of single grain monazite ages with published ages in the Southern Steep Belt. Partial melting of the Southern Steep Belt is contemporaneous with crystallization of the Bergell pluton and these melts may develop small dykes and stocks. Note the long time interval of partial melting in the SSB zone.

The significance of the ages for the Alpine orogen

Constraints on the time of residence of melt in the Southern Steep Belt are important to understand the geodynamic evolution in the tectonic accretion channel (TAC; Engi et al. 2001; Fig. 8) and to estimate the temporal range of the melt-induced strength decay of the crust at the time of deformation. U/Pb ages of aplites and pegmatites from the SSB cover a time span between 32 and 22 Ma (Romer et al. 1996; Schärer et al. 1996; Gebauer 1996). The analyzed, newly grown monazite grains in leucosomes of the metapelitic migmatites yield $^{207}Pb/^{235}U$ ages spreading between 28.10 ± 0.28 and 30.78 ± 0.14 Ma, i.e. consistent with previous investigations. These data indicate monazite formation within a time-span of at least 2.26 Ma between the youngest and oldest grain. Attributing the ages characterized by excess ^{206}Pb to crystallization from the melt, implies that melt was present in the migmatites over several million years, as previously inferred for the adjacent calc-alkaline Bergell pluton (Fig. 8; Oberli et al. 2004). This result suggests that long-term weakening was not restricted to the individual plutonic bodies, but to the entire migmatitic crust of the SSB.

Our new age data on the monazite of the metapelitic migmatites of the SSB can also be used to better constrain the timing of Barrovian metamorphism of the Central Alps. The investigated migmatites are part of a Barrovian metamorphic sequence (see Niggli 1970; Todd & Engi 1997; Fig. 8). Within the migmatites and their related aplites, the ages vary between 32 and 22 Ma (Hänny et al. 1975; Gebauer 1996; Schärer et al. 1996; Fig. 8). The aforementioned zircon SHRIMP data, monazite multi-grain analysis and the here presented monazite single-grain analysis overlap. This indicates that the SSB records possibly a long time interval (7–10 Ma) of high-grade metamorphic conditions including partial melting (see Burri et al. 2005 and Berger et al. 2008 for structural discussion).

Conclusions

The petrologic and microstructural investigation of migmatites with different bulk compositions showed that they formed by different melting reactions under similar P-T conditions. The described variable stability of accessory phases is related to the factors of chemical composition and water activity during crustal melting. The comparison of the accessory phases and

their textures in tonalitic and metapelitic migmatites shows that Ca activity exerts a major control on the stability of allanite versus monazite. Based on the inferred water contents of the rocks upon melting, we show that high water activity is also crucial for the stability of allanite under P-T conditions of 650–700 °C and 0.6–0.7 GPa (see also Fig. 6 of Janots et al. (2007)).

The present results shed some light on the criteria generally used to interpret isotopic ages measured on accessory mineral phases (e.g. monazite and allanite). If the H_2O and Ca activities of the protolith and the melt are similar, as in the anatexites of type 2 and 3, the relic accessory phases – and hence ages older than the melting event – are to be expected. In contrast, high water activity during melting leads to the growth of new accessory phases (monazites) at the expense of the older ones (allanites), and deletes the pre-melting isotopic age of the rock. Therefore, knowledge of the melting reactions and water activity of the anatexites may be of prime importance for the geological interpretation of isotopic ages of migmatites.

The present study also constrains the residence time of syntectonic partial melts in the Alpine crust of the SSB. The age data range from 30.78 ± 0.14 to 28.10 ± 0.28 Ma and are interpreted to constrain the occurrence of partial melts over more than two million years in the Southern Steep Belt of the Central Alps. The variation of data in one sample may also help to interpret the variation of literature data.

Acknowledgements

We thank the "Schweizerischer Nationalfonds" for supporting our research (200020-109637). Two anonymous reviewers helped to improve the quality of the manuscript. Edwin Gnos is thanked very much for editorial handling and for correcting the text. John Bailey is acknowledged for proof reading.

REFERENCES

Armbruster, T., Bonazzi, P., Akasaka, M., Bermanec, V., Chopin, C., Gieré, R., Heuss-Assbichler, S., Liebscher, A., Menchetti, S., Pan, Y. & Pasero, M., 2006: Recommended nomenclature of epidote-group minerals. European Journal of Mineralogy 18, 551–567.

Bea, F. & Montero, P., 1999: Behavior of accessory phases and redistribution of Zr, REE, Y, Th and U during metamorphism and partial melting of metapelites and partial melting of metapelites in the lower crust: An example from the kinzigite formation of Ivrea-Verbano, NW Italy. Geochemica Cosmochemica Acta 63, 1133–1153.

Berger, A., Rosenberg, C.L. & Schmid, S.M., 1996: Ascent, emplacement and exhumation of the Bergell Pluton within the Southern Steep Belt of the Central Alps. Schweizerische Mineralogische und Petrographische Mitteilungen 76, 357–382.

Berger, A. & Rosenberg, C.L., 2003: Preservation of chemical residue-melt equilibria in natural anatexite: the effects of deformation and rapid cooling. Contributions to Mineralogy and Petrology 144, 416–427.

Berger, A., Scherrer, N.C. & Bussy, F., 2005: Equilibration and disequilibration between monazite and garnet: indication from phase-composition and quantitative texture analysis. Journal of Metamorphic Geology 23, 865–880.

Berger, A., Burri, T., Alt-Epping, P. & Engi, M., 2008: Tectonically controlled fluid flow and water assisted melting in the middle crust: An example from the Central Alps. Lithos 102, 598–615.

Bingen, B. & van Breemen, O., 1998: U-Pb monazite ages in amphibolite- to granulite facies orthogneiss reflect hydrous mineral breakdown reactions: Sveconorwegian Province of SW Norway. Contributions to Mineralogy and Petrology 132, 336–353.

Broska, I., Petrik, I. & Williams, C.T., 2000: Coexisting monazite and allanite in peraluminous granitoids of the Tribec Mountains, Western Carpathians. American Mineralogist 85, 22–32.

Burri, T., 2005: From high-pressure to migmatisation: On orogenic evolution of the Southern Lepontine (Central Alps of Siwtzerland/Italy). Universität Bern, Bern, pp. 150.

Burri, T., Berger, A. & Engi, M., 2005: Tertiary migmatites in the Central Alps: Regional distribution, field relations, conditions of formation and tectonic implications. Schweizerische Mineralogische und Petrographische Mitteilungen 85, 215–232.

Büsch, W., Schneider, G. & Mehnert, K.R., 1974: Initial melting at grain boundaries. Part II: Melting in rocks of granodiorite, quartz diorite and tonalitic composition. Neues Jahrbuch für Mineralogie Monatshefte 8, 345–370.

Casillas, R., Nagy, G., Panto, G., Brandle, J. & Forizs, I., 1995: Occurrence of Th, U, Y, Zr and REE-bearing minerals in late Variscan granitic rocks from the Sierra Guadarrama (Spain). European Journal of Mineralogy 7, 989–1006.

Catlos, E.J., Sorenson, S.S. & Harrison, T.M., 2000: Th-Pb ion microprobe dating of allanite. American Mineralogist 85, 633–648.

Davidson, C., Rosenberg, C.L. & Schmid, S.M., 1996: Synmagmatic folding of the base of the Bergell pluton, Central Alps. Tectonophysics 265, 213–238.

Engi, M., Berger, A. & Roselle, G., 2001: The role of the tectonic accretion channel in collisional orogeny. Geology 29, 1143–1146.

Finger, F., Broska, I., Roberts, M.P. & Schermaier, A., 1998: Replacement of primary monazite by apatite-allanite-epidote coronas in an amphibolite facies granite gneiss from the Eastern Alps. American Mineralogist 83, 248–258.

Fitzsimonis, I.C.W., Kinny, P.D., Wetherley, S. & Hollingsworth, D.A., 2005: Bulk chemical control on metamorphic monazite growth in pelitic schists and implications for U/Pb age data. Journal of Metamorphic Geology 23, 261–277.

Förster, H.J., 1998: The chemical composition of REE-Y-Th-U-rich accessory minerals in peraluminous granites of the Erzgebirge-Fichtelgebirge region, Germany. Part II: Xenotime. American Mineralogist 83, 1302–1315.

Förster, H.J. & Harlov, D.E., 1999: Monazite-(Ce)-huttonite solid solutions in granulite-facies metabasites from the Ivrea-Verbano Zone, Italy. Mineralogical Magazine 63(4), 587–594.

Franz, G., Andrehs, G. & Rhede, D., 1996: Crystal chemistry of monazite and xenotime from Saxothuringian-Moldanubian metapelites, NE Bavaria, Germany. European Journal of Mineralogy 8, 1097–1118.

Gardien, V., Thompson, A.B. & Ulmer, P., 2000: Melting of biotite + plagioclase + quartz gneisses: the role of H_2O in the stability of amphibole. Journal of Petrology 41, 651–666.

Gebauer, D., 1996. A P-T-t Path for a high pressure ultramafic rock-associations and their felsic country rocks based on SHRIMP-Dating of magmatic and metamorphic zircon domains. Example: Alpe Arami (Central Swiss Alps). In: A. Hart & S.R. Basu (Editors), Earth Processes: Reading the Isotope Code, 307–328.

Hänny, R., Grauert, B. & Soptrajanova, G., 1975: Paleozoic migmatites affected by high grade Tertiary metamorphism in the Central Alps (Valle Bodengo, Italy): A geochronological study. Contributions to Mineralogy and Petrology 51, 173–196.

Hawkins, D.P. & Bowring, S.A., 1999: U-Pb monazite, xenotime and titanite geochronological constraints on the prograde to post-peak metamorphic thermal history of Paleoproterozoic migmatites from the Grand Canyon, Arizona. Contributions to Mineralogy and Petrology 134, 150–169.

Hermann, J., Rubatto, D. & Trommsdorff, V., 2006: Sub-solidus Oligocene zircon formation in garnet peridotite during fast decompression and fluid infiltration (Duria, Central Alps). Mineralogy and Petrology 88, 181–206.

Janots, E., Negro, F., Brunet, F., Goffé, B., Engi, M. and Bouybaouène, M.L., 2006: Evolution of the REE mineralogy in HP–LT metapelites of the Sebtide complex, Rif, Morocco: Monazite stability and geochronology. Lithos 87, 214–234.

Janots, E., Brunet, F., Goffé, B., Poinssot, C., Burchard, M. & Cemic, L., 2007: Thermochemistry of monazite-(La) and dissakisite-(La): implications for monazite and allanite stability in metapelites. Contributions to Mineralogy and Petrology 154, 1–14.

Janots, E., Engi, M., Berger, A., Allaz, J., Schwarz, O. & Spandler, C., 2008: Prograde metamorphic sequence of REE-minerals in pelitic rocks of the Central Alps: Implications on allanite – monazite – xenotime phase relations from 250° to 610 °C. Journal of Metamorphic Geology 26, 509–526.

Johannes, W. & Holtz, F., 1996: Petrogenesis and experimental petrology of granitic rocks. Springer, Berlin, 335 pp.

Kalt, A., Corfu, F. & Wijbrans, J.R., 2000: Time calibration of a P/T path from a Variscan high-temperature low-pressure metamorphic complex (Bayerische Wald, Germany), and the detection of inherited monazite. Contributions to Mineralogy and Petrology 138, 143–163.

Kelsey, D.E., Clark, C. & Hand, M., 2008: Thermobarometric modelling of zircon and monazite growth in melt-bearing systems: examples using model metapelitic and metapsammitic granulites. Journal of Metamorphic Geology 26, 199–212.

Köppel, V., Günthert, A. & Grünenfelder, M., 1981: Patterns of U–Pb zircon and monazite ages in polymetamorphic units of the Swiss Alps. Schweizerische Mineralogische und Petrographische Mitteilungen 61, 97–119.

Lee, D.E. & Silver, L.T., 1964: Accesory minerals in some granitic rocks in California and Nevada as a function of calcium content. American Mineralogist 49, 1660–1670.

Liati, A., Gebauer, D. & Fanning, M., 2000: U–Pb SHRIMP dating of zircon from the Novate granite (Bergell, Central Alps): evidence for Oligocene-Miocene magmatism, Jurassic/Cretaceous continental rifting and opening of the Valais trough. Schweizerische Mineralogische und Petrographische Mitteilungen 80, 305–316.

Miller, C.F. & Mittlefehldt, D.W., 1982: Depletion of light rare earth elements in felsic magmas. Geology 10, 129–133.

Mogk, D.W., 1992: Ductile shearing and migmatization at mid crustal levels in an Archean high grade gneiss belt, northern Gallatin range, Montana, USA. Journal of Metamorphic Geology 10, 427–438.

Nagel, T., 2000: Metamorphic and structural history of the Southern Adula nappe (Graubünden, Switzerland). PhD thesis, University of Basel, 103 pp.

Oberli, F., Meier, M., Berger, A., Rosenberg, C. & Gieré, R., 2004: $^{230}Th/^{238}U$ disequilibrium systematics in U-Th-Pb dating: Precise accessory mineral chronology and melt evolution tracing in the Alpine Bergell intrusion. Geochimica et Cosmochimica Acta 68, 2543–2560.

Peterson, R.C. & MacFarlane, D.B., 1993: The rare-earth-element chemistry of allanite from the Greenville province. Canadian Mineralogist 31, 159–166.

Petrik, I., Broska, I., Lipka, J. & Siman, P., 1995: Granitoid allanite-(Ce): Substitution relations, redox conditions and REE distrubutions (on the example of I-type granitoids, Western Carpathians, Slovakia). Geologica Carpathica 46, 79–94.

Poitrasson, F., 2002: In situ investigations of allanite hydrothermal alteration: examples from calc-alkaline and anorogenic granites of Corsica (Southeast France). Contributions to Mineralogy and Petrology 142, 485–500.

Pyle, J.M. & Spear, F.S., 2000: An empirical garnet (YAG) – xenotime thermometer. Contributions to Mineralogy and Petrology 138, 51–58.

Pyle, J.M. & Spear, F.S., 2003: Four generations of accessory-phase growth in low-pressure migmatites from SW New Hampshire. American Mineralogist 88, 338–351.

Pyle, J.M., Spear, F.S., Rudnick, R.L. & McDonough, W.F., 2001: Monazite-xenotime-garnet equilibrium in metapelites and a new monazite-garnet thermometer. Journal of Petrology 42, 2083–2107.

Rasmussen, B., Muhling, J.R., Fletcher, I.R. & Wingate, M.T.D., 2006: In situ SHRIMP U-Pb dating of monazite integrated with petrology and textures: Does bulk composition control whether monazite forms in low-Ca pelitic rocks during amphibolite facies metamorphism? Geochimica et Cosmochimica Acta 70, 3040–3058.

Romer, R.L., Schärer, U. & Steck, A., 1996: Alpine and pre-Alpine magmatism in the root-zone of the western Central Alps. Contributions to Mineralogy and Petrology 123, 138–158.

Rosenberg, C.L., Medvedev, S. & Handy, M., 2007: Effects of melting on faulting and continental deformation. In: M. Handy, G. Hirth & N. Hovius (Eds.), Tectonic Faults: Agents of Change on a Dynamic Earth. MIT Press, 357–402.

Rosenberg, C.L. & Berger, A., 2001: Syntectonic melt pathways in granitic gneisses, and melt-induced transition in deformation mechanisms. Physics and Chemistry of the Earth 26, 287–293.

Rosenberg, C.L., Berger, A. & Schmid S.M., 1995: Observation on the floor of a granitoid pluton; inferences on the driving force of final emplacement. Geology 23, 443–446.

Rubatto, D., Williams, I.S. & Buick, I.S., 2001: Zircon and monazite response to prograde metamorphism in the Reynolds Range, central Australia. Contributions to Mineralogy and Petrology 140, 458–468.

Schaltegger, U., Pettke, T., Audat, A., Reusser, E. & Heinrich, C.A., 2005: Magmatic-to-hydrothermal crystallization in the W-Sn mineralized Mole Granite (NSW, Australia). Part I: Crystallization of zircon and REE-phosphates over three million years – a geochemical and U-Pb geochronological study. Chemical Geology 220, 215–235.

Schärer, U., 1984: The effect of initial ^{230}Th disequilibrium on young U-Pb ages; the Makalu case, Himalaya. Earth and Planetary Science Letters 67, 191–204.

Schärer, U., Cosca, M., Steck, A. & Hunziker, J., 1996: Termination of major ductile strike slip shear and differential cooling along the Insubric line (Central Alps): U-Pb, Rb-Sr and Ar/Ar ages of cross-cutting pegmatites. Earth and Planetary Science Letters 142, 331–351.

Scherrer, N.C., Engi, M., Gnos, E., Jakob, V. & Liechti, A., 2000: Monazite analysis; from sample preparation to microprobe age dating and REE quantification. Schweizerische Mineralogische und Petrographische Mitteilungen 80, 93–105.

Schmidt, M. & Thompson, A.B., 1996: Epidote in calc-alkaline magmas: An experimental study of stability, phase relationships, and the role of epidote in magmatic evolution. American Mineralogist 81, 762–474.

Smith, H.A. & Barreiro, B., 1990. Monazite U-Pb dating of staurolite grade metamorphism in pelitic schists. Contributions to Mineralogy and Petrology, 105, 602–615.

Stacey, J.S. & Kramers, J.D., 1975: Approximation of terrestrial lead isotope evolution by a two-stage model. Earth and Planetary Science Letters 26, 207–221.

Todd, C.S. & Engi, M., 1997: Metamorphic field gradients in the Central Alps. Journal of Metamorphic Geology 15, 513–530.

Tomkins, H.S. & Pattison, D.R.M., 2007. Accessory phase petrogenesis in relation to major phase assemblages in pelites from the Nelson contact aureole, southern British Columbia. Journal of Metamorphic Geology 25, 401–421.

Trommsdorff, V. & Conolly, J., 1996: The ultramafic contact aureole about the Bregaglia (Bergell) tonalite: Isograds and a thermal model. Schweizerische Mineralogische und Petrographische Mitteilungen 76, 537–547.

Vance, D. & O'Nions, R.K., 1992: Prograde and retrograde thermal histories from the Central Swiss Alps. Earth and Planetary Science Letters 114, 113–129.

Watt, G.R., Burns, I.M. & Graham, G.A., 1996: Chemical charateristics of migmatites: accessory phase distrubution and evidence for fast melt segregation. Contributions to Mineralogy and Petrology 125, 100–111.

Wing, B.A., Ferry, J.M. & Harrison, T.M., 2003: Prograde destruction and formation of monazite and allanite during contact and regional metamorphism of pelites: petrology and geochronology. Contributions to Mineralogy and Petrology 145, 228–250.

Wood, S.A. & Ricketts, A., 2000: Allanite-(Ce) from the Eocene Casto Granite, Idaho; response to hydrothermal alteration. Canadian Mineralogist 38, 81–100.

Manuscript received October 25, 2007
Revision accepted December 1, 2008
Published Online first February 14, 2009
Editorial Handling: Edwin Gnos

Appendix

Allanites are solid solutions of epidote group minerals with the general formula: $(Ca,REE,Th)_2(Fe^{2+},Fe^{3+},Al,Ti)_3Si_3O_{12}(OH)$. For a more complete discussion, see also Armbruster et al. (2006). We describe allanites using clinozoisite ($Ca_2Al_2AlOHSi_3O_{12}$) as end-member composition and define the following components:

Ferriepidote	$Ca_2\ Fe^{3+}\ Al_2OHSi_3O_{12}$
Allanite	$Ca\ REE\ Fe^{2+}\ Al_2OHSi_3O_{12}$
Th-component	$Th\ Al\ Al_2OHSi_3O_{12}$

$X_{REE} = D/A$
$X_{Th} = Th/A$

where:

$D = Y + La + Ce + Pr + Nd + Sm + Gd + Dy + Ho + Er$
$A = Ca + Mn + Sr + Y + La + Ce + Pr + Nd + Sm + Gd + Dy + Ho + Er + Pb + Th$

The main exchange vectors for the REE are coupled substitutions affecting the A- and M-sites: $Ca + (Al, Fe^{3+}) = REE + Fe^{2+}$ (e.g., Petrik et al. 1995).

Therefore, we use:

$X_{Czo} = Al/(Al + Mg + Ti + Fe^{2+} + Fe^{3+})$
$X_{Ferriep} = Fe^{3+}/(Al + Mg + Ti + Fe^{2+} + Fe^{3+})$
$X_{Fe2+} = Fe^{2+}/(Al + Mg + Ti + Fe^{2+} + Fe^{3+})$

The $X_{Fe^{2+}}$ is directly connected to the amount of REE, if no dissakisite component is present. Other important components in epidote group minerals (Mn, Cr, V, etc) were ignored in this study.